ELSEVIER

Urologic Oncology: Seminars and Original Investigations 37 (2019) 573.e19–573.e29

UROLOGIC ONCOLOGY

Laboratory-Bladder cancer

Morphologic and genomic characterization of urothelial to sarcomatoid transition in muscle-invasive bladder cancer

Vera Genitsch, M.D.[a,1], Attila Kollár, M.D.[b,1], Gillian Vandekerkhove, M.Sc.[c], Jennifer Blarer, M.D.[d], Marc Furrer, M.D.[d], Matti Annala, M.Sc.[c,e], Cameron Herberts, B.Sc.[c], Armin Pycha, M.D.[f], Joep J. de Jong, B.Sc.[h], Yang Liu, Ph.D.[g], Friedemann Krentel, M.D.[c], Elai Davicioni, Ph.D.[g], Ewan A. Gibb, Ph.D.[g], Marianna Kruithof-de Julio, Ph.D.[d], Alexander W. Wyatt, Ph.D.[c], Roland Seiler, M.D.[d,*]

[a] *Institute of Pathology, University of Bern, Switzerland*
[b] *Department of Medical Oncology, Inselspital, Bern University Hospital, University of Bern, Switzerland*
[c] *Vancouver Prostate Centre and Department of Urologic Sciences, University of British Columbia, Vancouver, Canada*
[d] *Department of Urology, Inselspital, Bern University Hospital, University of Bern, Switzerland*
[e] *Faculty of Medicine and Health Technology, Tampere University, Tampere, Finland*
[f] *Department of Urology, Central Hospital of Bolzano, Bolzano, Italy*
[g] *GenomeDx Inc., Vancouver, Canada*
[h] *Department of Urology, Erasmus MC Cancer Institute, Rotterdam, The Netherlands*

Received 4 March 2019; received in revised form 22 June 2019; accepted 23 June 2019

Abstract

Introduction: The sarcomatoid morphology of muscle-invasive bladder cancer (MIBC) is associated with unfavorable prognosis. However, the genomic, transcriptomic, and proteomic relationship between conventional urothelial and synchronous sarcomatoid morphology is poorly defined.

Methods: We compiled a cohort of 21 MIBC patients with components of conventional urothelial and adjacent sarcomatoid morphology within the same tumor focus. We performed comprehensive pathologic and immunohistochemical characterization and in 4 selected cases, subjected both morphologic components to targeted DNA sequencing and whole transcriptome analysis.

Results: Synchronous sarcomatoid and urothelial morphology from the same MIBC foci shared truncal somatic mutations, indicating a common ancestral clone. However, additional mutations or copy number alterations restricted to the either component suggested divergent evolution at the genomic level. This was confirmed at the transcriptome level since while the urothelial component exhibited a basal-like subtype (TCGA2014: cluster III, LundTax: basal/squamous-like), the sarcomatoid morphology was predominantly cluster IV (claudin-low). Protein expression was consistent with a basal-like phenotype in both morphologies in 18/21 of cases. However, most cases had evidence of active epithelial-to-mesenchymal transition (E-Cad ↓ and Zeb1 or TWIST1 ↑) from urothelial toward the sarcomatoid morphology. Drug response signatures nominated different targets for each morphology and proposed agents under clinical investigation in liposarcoma or other sarcoma. PD-L1 expression was higher in the sarcomatoid than the urothelial component.

Conclusions: Conventional urothelial and adjacent sarcomatoid morphologies of MIBC arise from the same common ancestor and share a basal-like phenotype. However, divergence between the morphologies at the genome, transcriptome, and proteome level suggests differential sensitivity to therapy.

Keywords: Muscle-invasive bladder cancer; Sarcomatoid variant; Molecular subtypes; Epithelial-to-mesenchymal transition

*Corresponding author. Tel.: +41764381118; fax: +41316322181.
E-mail addresses: r_seiler@gmx.ch, roland.seiler@insel.ch (R. Seiler).
[1]Contributed equally.

https://doi.org/10.1016/j.urolonc.2019.06.021

1. Introduction

Muscle-invasive bladder cancer (MIBC) is a heterogeneous disease with a highly variable clinical prognosis. Approximately 50% of the patients die within 5 years after diagnosis despite best standard of care [1], 35% of advanced tumor stage patients with pelvic lymph node metastases are still long term survivors [1,2]. Response to systemic treatment regimen also varies, with less than 30% of patients deriving a benefit from cisplatin-based regimens [3] or immune checkpoint inhibition [4].

This clinical heterogeneity is underlined by remarkably high inter- [5,6] and intratumoral genomic heterogeneity [7,8]. Morphological divers tumors may show a plasticity in tumor subtypes [8]. MIBC shows a significant range of pathological morphologies and indeed, 12 distinct histological variants in addition to conventional urothelial morphology have been characterized [9]. Different morphologies are associated with different clinical courses [10,11] and responsiveness to systemic treatments [12,13]. However, our understanding of the relationship between genomic, biologic, and morphologic characteristics is only partially complete. The micropapillary morphology frequently harbors alterations in the Her2 signaling pathway [14–16], while the plasmocytoid morphology is characterized by a frequent somatic loss of *CDH1* [17]. The squamous variant is enriched in basal-like MIBCs [8,36]. Warrick et al. [18] investigated characteristics of several morphologies including squamous, glandular, micropapillary, nested, plasmacytoid, and sarcomatoid. Interestingly, although the latter is associated with unfavorable prognosis [19–21] and a link with a specific molecular genotype or phenotype has not been established [18]. Sarcomatoid morphology is often concomitant to conventional urothelial MIBC and foci of both morphological growth patterns may merge in the same tumor focus [19]. Therefore, biological characteristics of the sarcomatoid morphology may best be elucidated by investigating urothelial MIBC and the adjacent transition into sarcomatoid morphology within the same MIBC focus [22–24]. Prior studies have examined a small number of genomic markers such as TP53 mutation status or microsatellite polymorphism and concluded that the 2 morphologies are likely monoclonal [22–24]. However, a comprehensive genomic analysis has not been performed, and furthermore, no study has linked the genome, transcriptome, and proteome of sarcomatoid and adjacent urothelial MIBC to dissect tumor heterogeneity and the implications for treatment strategy.

2. Patients and Methods

2.1. Cohort selection and pathological review

Between 2002 and 2014, 21 patients without prior neoadjuvant chemotherapy or BCG instillation therapy underwent standardized extended bilateral pelvic lymphadenectomy with cystectomy for urothelial carcinoma of the bladder at the Department of Urology, University of Bern. Histological re-evaluation by an experienced uropathologist (VG) confirmed that these patients showed conventional urothelial and adjacent sarcomatoid morphology. The use of patient material for this study was approved by the local human research ethics board (protocol number: Bern, Switzerland KEK-No. 2017-01566). All cases were used to generate a tissue microarray (TMA, Fig. 1A). Four cases were selected for DNA sequencing and an additional four 1 mm cores were taken from formalin fixed paraffin embedded (FFPE) tissue regions representing each of the urothelial and sarcomatoid morphologies in these cases (Fig. 1B, Supplementary Fig. 1). In 2 of these cases, pelvic lymph node metastases collected during cystectomy were also sampled for genomic profiling.

2.2. Targeted DNA sequencing

DNA was extracted from FFPE tissue samples using the Promega Maxwell RSC instrument and DNA FFPE kit; quantification was performed on the Quantus Fluorometer via the QuantiFluor ONE dsDNA System. We employed an established targeted sequencing strategy capturing the exonic regions of 50 genes frequently associated with bladder cancer (Supplementary Table 1; Supplementary Methods) [25–27]. Sequence data analysis, including identification of somatic mutations, copy number alterations, and structural rearrangements was performed exactly as previously described [25–27]. Note that although mutations were called independently in each sample using our established approach, for instances where a mutation was not identified in all samples from a patient, we reviewed sequence read support for that mutation in each sample as a secondary analysis.

2.3. Gene expression analysis

Whole transcriptome profiling was performed with the Decipher assay (based on the Human Exon 1.0 ST oligonucleotide microarray) in a CAP/CLIA clinical laboratory (GenomeDx, Inc, San Diego, CA) [28]. We selected 16 cores (8 urothelial and 8 sarcomatoid) from 4 cases for analysis. To describe the degree of transcriptomic heterogeneity within a given morphology, we compared cores from the same area. To compare morphologies (urothelial vs. sarcomatoid) we used the median gene expression levels from all cores of the respective morphology.

To generate RNA molecular subtypes we first assimilated gene expression profiles with our previously published dataset [29]. We then used published methods [6,30] as well as the consensus classifier [31] of The Bladder Cancer Molecular Taxonomy Group, to generate subtype calls across the entire dataset.

Unsupervised consensus clustering, principal component analysis, and gene set enrichment analysis was performed (Supplementary methods).

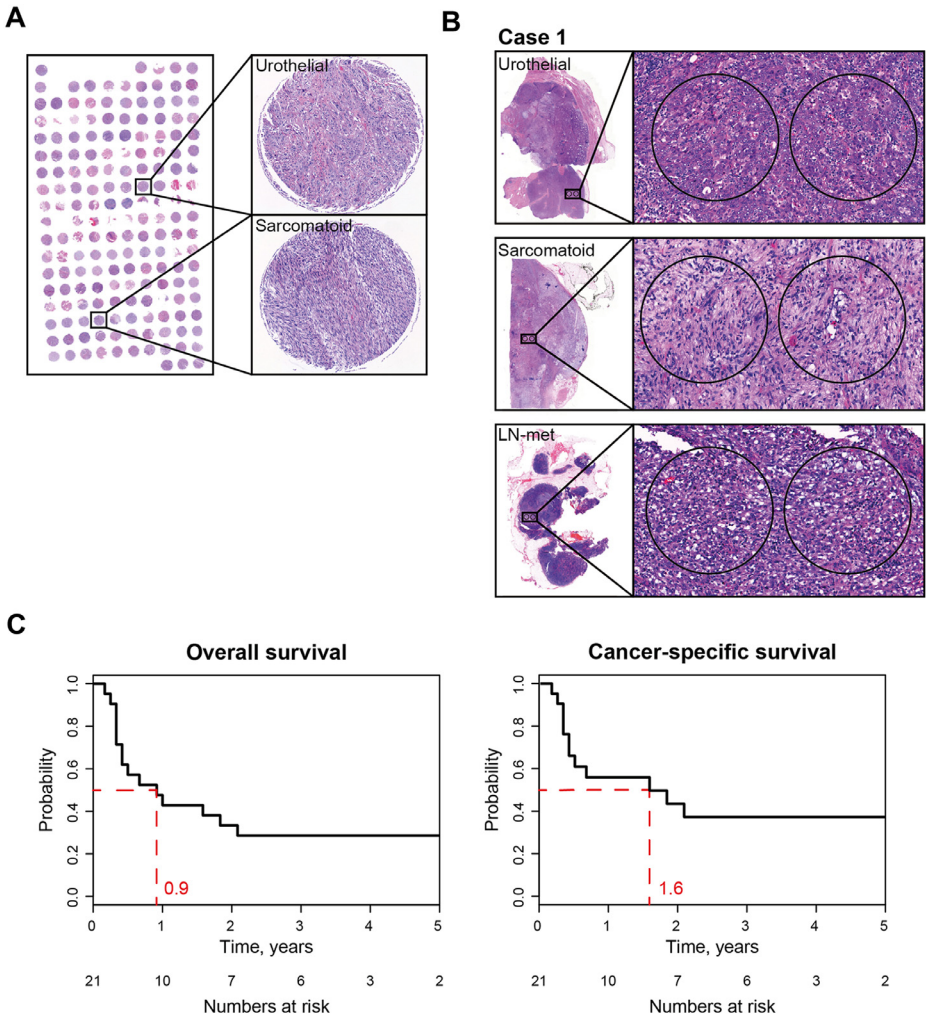

Fig. 1. Outcome and pathological characteristics. (A) A TMA was constructed of all cystectomy specimens by sampling 2 respectively 4 cores of the urothelial (if present) and sarcomatoid morphology. (B) Four cases were additionally sampled for genomic and transcriptomic analyses. In Cases 1 and 2, corresponding lymph node metastases were sampled as well. (C) Kaplan-Meier plot for overall (left) and cancer-specific survival (right) of the 21 patients.

2.4. Calculation of drug response scores

The CellMiner tool was used to identify drug response related genes from data derived from the NCI-60 cell line panel [32]. Corresponding genes were used to generate patient specific drug response scores (DRS) using correlation coefficients as weighting factors.

2.5. TMA constructions and immunohistochemistry

A TMA was constructed as previously published [33]. 2 (urothelial) and 4 (sarcomatoid) 1-mm cores were sampled from each morphology. Immunohistochemical staining for CK5/6, GATA3, CD44, E-cadherin, Zeb1, TWIST1, PD-L1 (SP263), FoxP3, and CD8 expression was performed using a Leica Bond or Ventana Benchmark Ultra automated immunostainer. PD-L1 staining was scored according to the manufacturer's guidelines for urothelial carcinoma.

3. Results

3.1. Baseline patient characteristics and outcome

Clinicopathological characteristics of the patients are provided in Table 1. Median overall and cancer specific survival of the cohort were 0.9 and 1.6 years, respectively (Fig. 1C).

3.2. Morphological characteristics

The vast majority of sarcomatoid tumor regions exhibited classical spindle cell morphology. Additional morphologic variants in other areas of the tumors included squamous differentiation (10/21 cases), glandular (2/21), or focal clear cell or micropapillary differentiation (1 case each). Carcinoma in situ could be observed in 17/21 cases, while only 2/21 tumors showed papillary morphology.

Table 1
Clinicopathological characteristics of the patients.

Patient characteristics	$n = 21$
Median age (range), y	72 (30−86)
Gender, *n* (%)	
Female	6 (29)
Male	15 (71)
Median follow-up, y (range)	4.3 (0.2−14)
Tumor stage and histology	
T-stage, *n* (%)	
pT ≤ 2	2 (10)
pT3/4	19 (90)
N-stage, *n* (%)	
pNX	2 (10)
pN0	11 (52)
pN+	8 (38)
Lymphangiosis, *n* (%)	14 (66)
Hemangiosis, *n* (%)	16 (80)
Perineural invasion, *n* (%)	13 (62)
Lymph nodes, *n* (range)	
Examined	37 (0−80)
Positive	0 (0−7)
Postoperative therapy	
Radiotherapy, *n* (%)	5 (24)
Chemotherapy, *n* (%)	6 (29)

3.3. Adjacent urothelial and sarcomatoid morphology arise from a shared ancestral clone

We performed targeted deep sequencing of 4 pairs of synchronous urothelial and sarcomatoid morphology. In 2 cases, metastases to local lymph nodes were also profiled. In all cases, nonmalignant lymph node tissue was used as germline control. Median sequencing depth across tumor tissue was 286×.

In all 4 pairs, the morphologies shared somatic mutations and copy number changes, indicating a common ancestral clone (Fig. 2; Supplementary Table 2). However, we also detected alterations that were unique to each morphology in 3 of 4 cases (Fig. 2A−C; Supplementary Table 2). Some morphology-restricted mutations were present at high allele fractions, suggesting they were fixed in their respective tumor cell population; a notable example was a missense mutation in *FGFR3* that was present at 54% in the urothelial component of Case 1 but below detection thresholds in the sarcomatoid morphology. Similarly, the urothelial component of Case 2 harbored a high level *CCND1* amplification that was absent from the sarcomatoid component. Together these data suggest divergent evolution between the urothelial and sarcomatoid morphologies, despite the overall ancestral relationship. In the 2 cases where lymph node metastases were profiled, high copy number concordance and shared somatic mutations indicated strong similarity to the primary sarcomatoid morphology in Case 1 and to the primary urothelial morphology in Case 2 (Fig. 2B−C; Supplementary Fig. 2). Overall, all genomic alterations were consistent with aggressive MIBC (Fig. 2A−D). For example, all 4 cases had truncal *TP53* and/or *RB1* mutations, often accompanied by loss of heterozygosity or a second inactivating mutation, and all were shared between both morphologies.

3.3.1. Concordance of genomic alterations with gene expression

Differences in copy number variations (*FGFR1*, *CCND1,* and *CDKN2A*) between urothelial and sarcomatoid morphology of Case 1 were reflected by differences in corresponding transcript expression levels (Fig. 2D). Similar concordance was observed in other cases, including an *ERBB2* amplification with *ERBB2* transcript upregulation, and a *TSC2* deletion with concomitant transcriptional downregulation.

3.4. Gene expression analysis reveals heterogeneity between both morphologies

All but one sample (Sarcomatoid Case 1) passed quality control. There was a high correlation for global transcription profiles between different regions of the same morphology (Fig. 3A). In all but one case, each pair had a correlation coefficient of 0.94 or higher (Pearson). However, the correlation coefficient was lower for comparisons between morphologies within a patient (median *R*-values: 0.94 vs. 0.9, $P = 0.069$, Wilcoxon).

These findings were supported by IHC across the entire cohort (Fig. 3B). CD44 and PD-L1 protein expression levels were significantly positive correlated within each morphology but not when compared between urothelial and sarcomatoid.

3.5. Urothelial and sarcomatoid morphology have a basal-like consensus RNA molecular subtype

Consensus mRNA-based subtyping suggested that in the vast majority of cases both morphologic variants fell within the basal-like classification (Fig. 4A). However, although the urothelial foci were generally classified as basal/squamous-like (Ba/Sq, LundTax, and Consensus) or Cluster III (TCGA 2014), the sarcomatoid regions had features consistent with an additional invasive component (Ba/Sq-Inf; Cluster IV, Mes-like, Stroma-rich). At the RNA level, the expression of basal cytokeratins (*KRT5*, *KRT6*) was higher in the urothelial compared to sarcomatoid morphology, but the expression level of *CD44*, a basal stem cell marker, was virtually identical (Fig. 4B). Protein expression analysis across the entire cohort confirmed these findings: 12/19 cases presented with a more extensive CK5/6 expression in the urothelial component compared to the sarcomatoid morphology, while CD44 was positive in both regions in 15/19 cases (Fig. 4C).

Pathway and gene set enrichment analysis suggested that features of epithelial-to-mesenchymal transition were significantly enriched in the sarcomatoid compared to the urothelial morphology (Fig. 4D). This was consistent at the protein level in most cases, where E-cadherin decreased

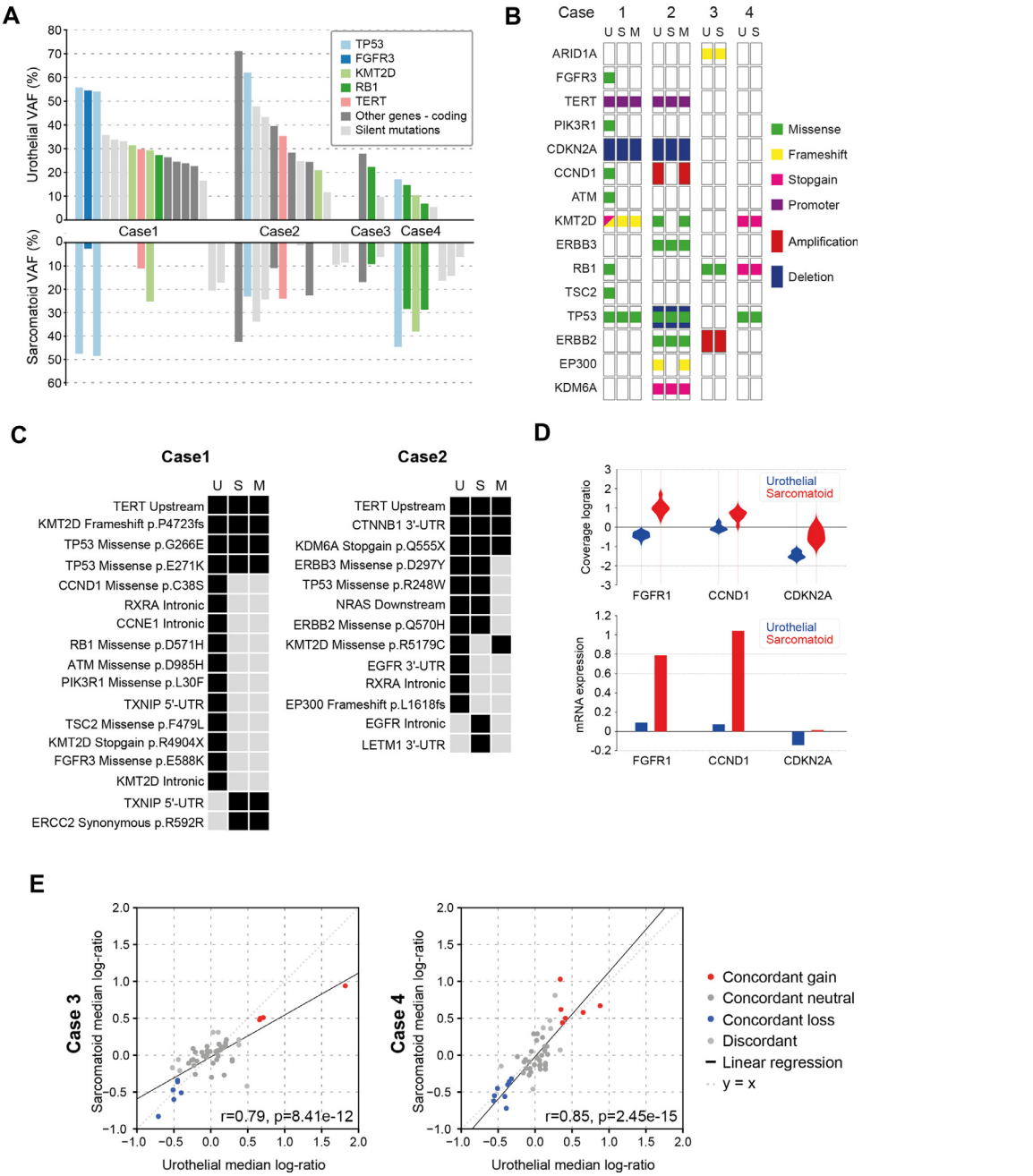

Fig. 2. Adjacent urothelial and sarcomatoid morphologies arise from a shared common ancestor. (A) Mirror plot indicating the variant allele frequency (VAF) of somatic mutations detected in both the urothelial (top) and sarcomatoid (bottom) morphologies for 4 cases subjected to targeted DNA sequencing. (B) Genomic alterations detected in the urothelial (U) and sarcomatoid (S) morphologies, and lymph node metastases (M) of 4 cases. Select copy-number alterations are shown. Note that a distinction is not made between hemizygous and homozygous deletions. (C) Mutations are shared or morphology-specific. Comparison of mutations detected in the urothelial (U) and sarcomatoid (S) morphologies, and lymph node metastases (M), of Cases 1 and 2. (D) Concordance of copy number coverage log ratio from targeted DNA sequencing and mRNA expression levels in Case 1. (E) Copy number calls are highly correlated between urothelial (*x*-axis) and sarcomatoid (*y*-axis) morphologies in Cases 3 and 4 (linear least squares regression).

and/or TWIST1, ZEB1 increased when moving from the urothelial to the sarcomatoid morphology (Fig. 4E).

3.6. Impact on treatment strategies

We applied linear models to calculate DRS for 89 drugs. The higher the score for a given drug, the more promising the treatment success in this given tumor. DRS clustered urothelial and sarcomatoid morphology (Fig. 5A). While DRS of some drugs were higher in urothelial morphology (Dolastatin, Docetaxel), other drugs, investigated for treatment of sarcoma, were higher in sarcomatoid morphology (Lovastatin, Rebimastat, Triapine), respectively (Fig. 5A).

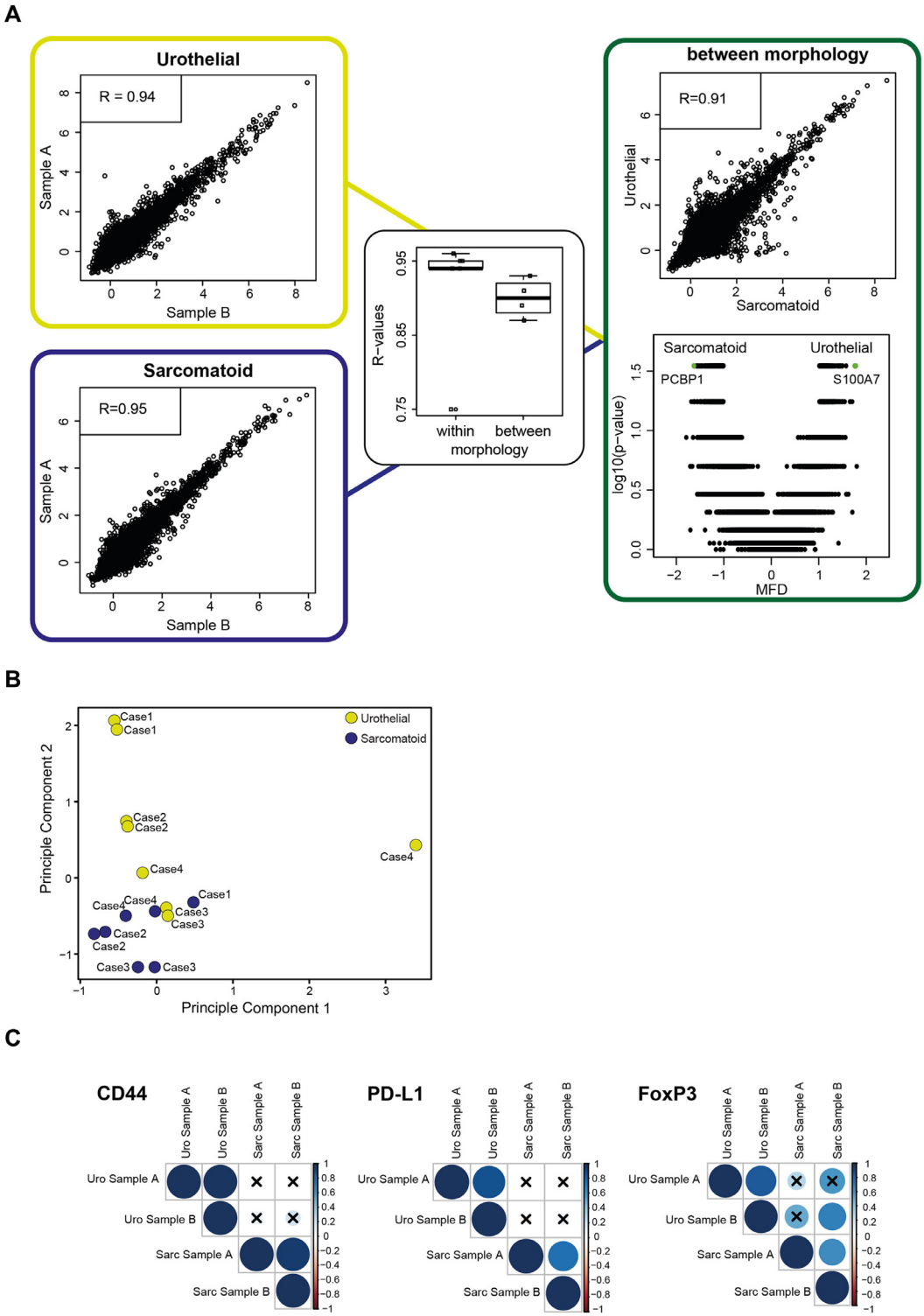

Fig. 3. Expression data on tumor heterogeneity between both morphologies. (A) Heterogeneity within and between both morphologies. Gene expression between 2 areas within the same morphology showed a high correlation (correlation plots on the left, Pearson). This correlation decreased when gene expression between both morphologies was compared (correlation plot on the right, Pearson). In $^{3}/_{4}$ cases, *R*-values decreased when comparing gene expression within and between the morphologies, respectively (boxplot in the middle, Wilcoxon). In addition, volcano plot indicates differences in gene expression between both morphologies. Genes associated with a basal-like phenotype (such as S100A7) were overexpressed in the urothelial morphology. (B) Principal component analysis on all individual samples passing quality control. With the exception of urothelial Case 4, all samples from the same case and morphology grouped together and away from the samples of the other morphology. (C) Correlation of selected markers analyzed by IHC in the TMAs between 2 areas within the same morphology and between 2 areas to the other morphology (Pearson). The larger the point, the higher the correlation. Blue and red for a positive and negative correlation, respectively. The cross indicates a nonsignificant correlation. "Color version available online."

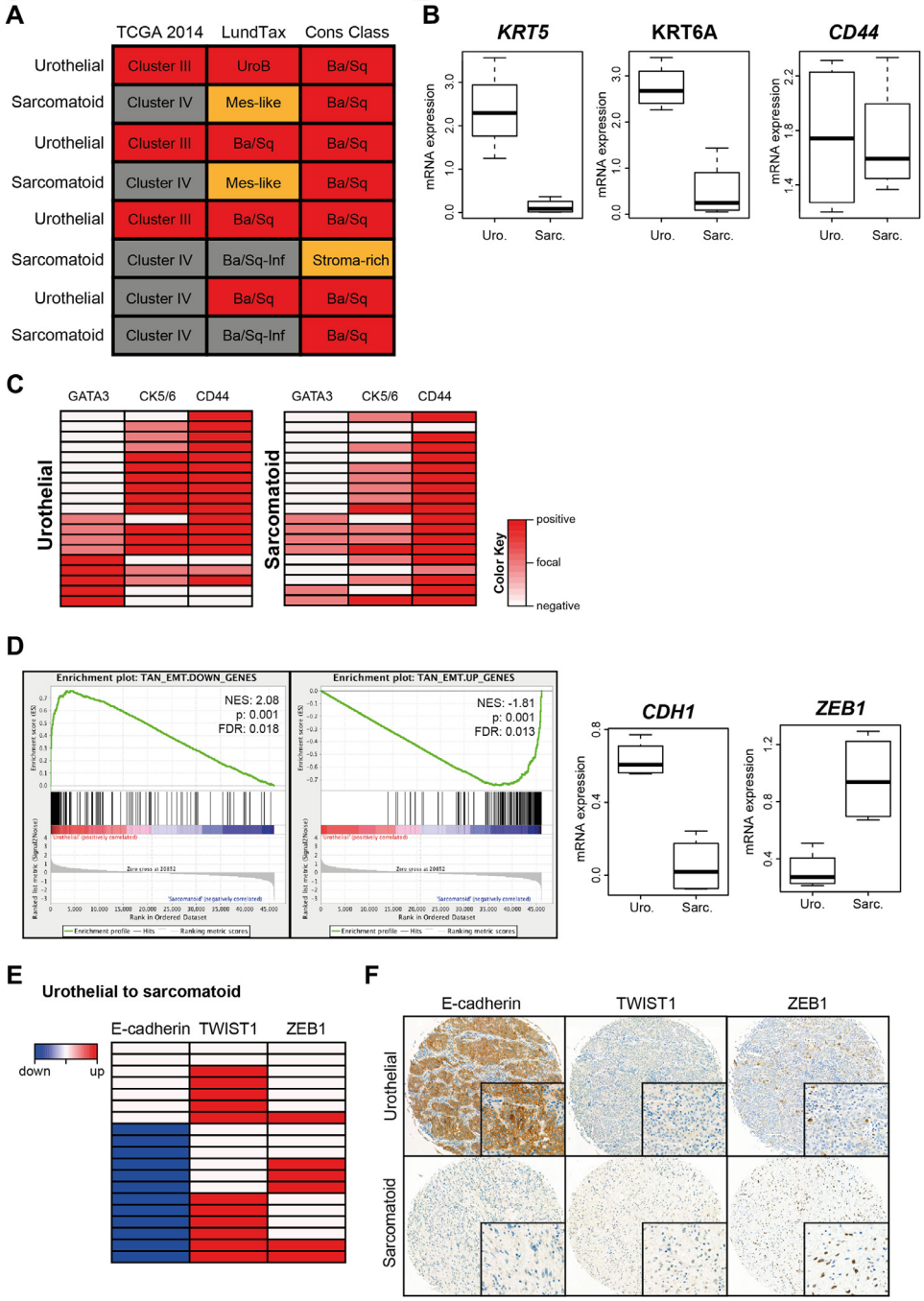

Fig. 4. Molecular subtyping and pathway analysis. (A) Subtype calls in both morphologies using the TCGA2014, LundTax, and Consensus molecular subtyping classifiers. (B) Gene expression of basal cytokeratins (*KRT5*, *KRT6*) and *CD44* in urothelial and sarcomatoid morphology. (C) Investigating molecular phenotype using IHC (GATA3, CK5/6 and CD44), a basal-like phenotype was assigned in both components in 16/19 cases. (D) Bidirectional signatures for epithelial-to-mesenchymal transition indicate a significant enrichment of the sarcomatoid morphology for EMT, when compared to the urothelial morphology. This is underlined by the higher and lower expression of *ZEB1* and *CDH1*, respectively. Enrichment of EMT in sarcomatoid morphology, when compared to urothelial. (E) This heatmap indicates the IHC analysis of EMT from the urothelial to the sarcomatoid morphology. E-cadherin and TWIST1/ZEB1 were frequently under- and overexpressed toward sarcomatoid morphology, respectively. Under- and overexpression from the urothelial to the sarcomatoid morphology are given in blue and red, respectively. (F) Representative case with loss of E-cadherin and increasing TWIST1/ZEB1 expression from urothelial to sarcomatoid morphology. "Color version available online."

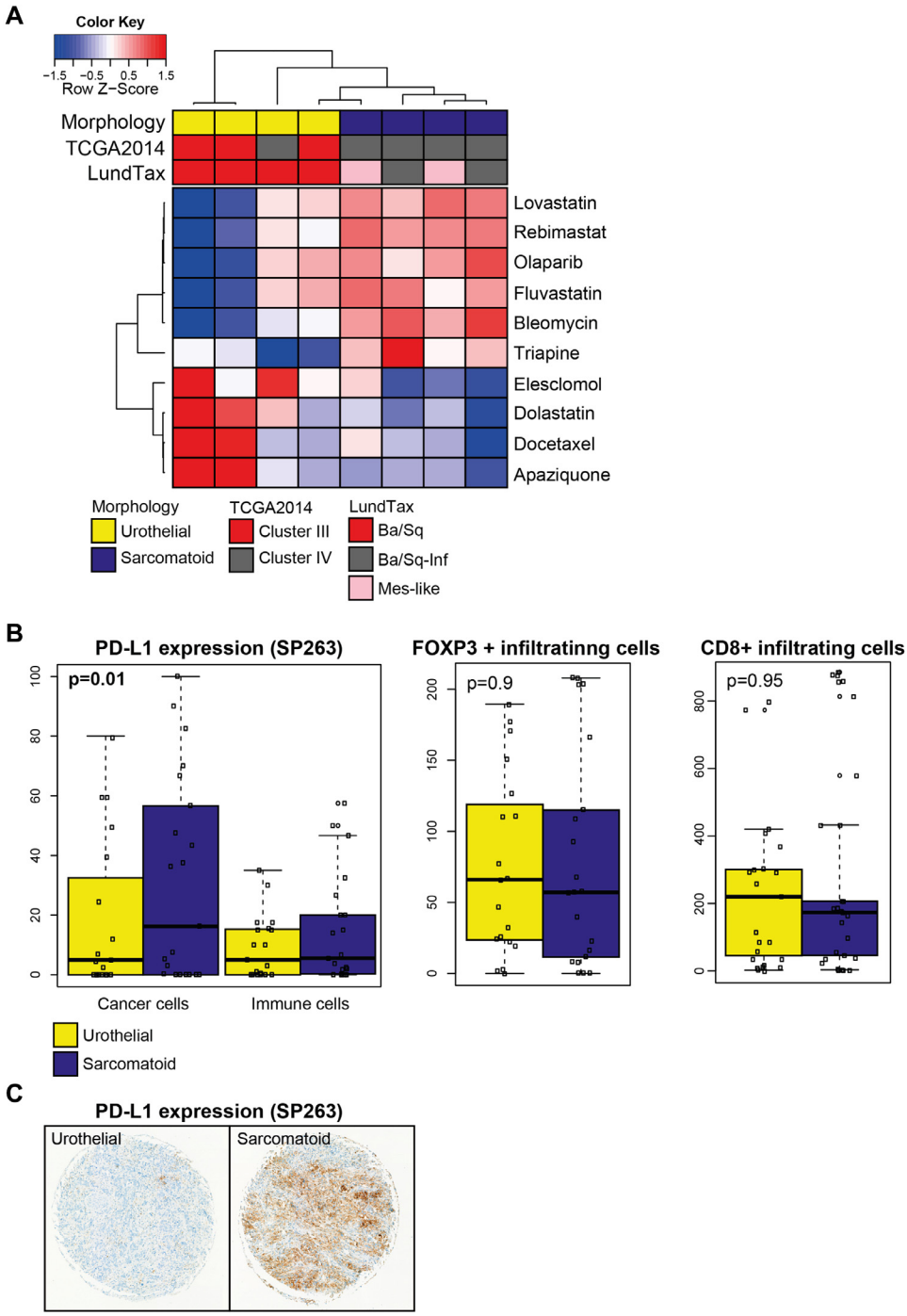

Fig. 5. Impact on treatment strategies. (A) Heatmap of drug response scores calculated for the urothelial and sarcomatoid components of 4 tumors. The top covariate track indicates the urothelial (yellow) and sarcomatoid (blue) components, respectively. A covariate track for the subtype assignments for both TCGA2014 and LundTax classifiers is also provided. The drugs with a higher score (red) suggest higher sensitivity compared to a lower score (blue). (B) Expression of PD-L1 in cancer and immune cells, number of FoxP3 and CD8 expressing tumor infiltrating lymphocytes between urothelial and sarcomatoid morphology, respectively (Wilcoxon). PD-L1 expression was significantly higher in the sarcomatoid morphology when compared to urothelial. Number of FoxP3 and CD8 positive tumor infiltrating lymphocytes remained approximately the same (Wilcoxon). (C) Urothelial and sarcomatoid components of a representative case stained with PD-L1 (SP263). "Color version available online."

PD-L1 expression in cancer cells and immune cells significantly increased from the urothelial to the sarcomatoid morphology, while the number of FoxP3 and CD8 expressing lymphocytes remained approximately the same (Fig. 5B and C).

4. Discussion

In this study, we describe the phenotype of a cohort of 21 patients with conventional urothelial MIBC and adjacent sarcomatoid morphology and defined the molecular

landscape of a selected group of cases. Our findings were consistent across the cohort: (i) both morphologies arise from a common ancestor; (ii) the majority of urothelial and adjacent sarcomatoid MIBC have a basal-like phenotype but molecular heterogeneity between morphologies is prominent; (iii) there is strong evidence for epithelial-to-mesenchymal transition from the urothelial to the sarcomatoid morphology; and (iv) different compounds may be required for successful treatment of both the urothelial and the adjacent sarcomatoid morphology.

Tumors with both urothelial and sarcomatoid morphology showed genomic DNA alterations that are frequent in bladder cancer such as mutations or deletions in KMT2D, TP53, and RB1, respectively [5]. In line with previous data [22,23], our findings suggest that both morphologies arise from the same common ancestor. The mechanism or process by which the pathologic divergence occurs remains unclear. It is interesting to note that loss of TP53 and RB1 is linked with cellular plasticity in other cancers [34,35], however alterations to these genes are also common in conventional MIBC. We can only hypothesize that loss of these tumor suppressors can also promote a shift toward sarcomatoid morphology. However, we found differences in the genomic landscape between both and could assign corresponding lymph node metastases to derive from one or the other morphology, respectively. Although being from the same common ancestor, this genomic heterogeneity may impact strategies for successful treatment.

We further elucidated transcriptomic heterogeneity between both morphologies, although application of different methods for molecular subtyping suggested that almost all were broadly basal-like [6,30,31]. This is supported by the frequent loss of RB1 observed at the genomic level in this study, and the fact that only 3/21 tumors did not express proteins consistent with a basal-like phenotype. Furthermore, only 2/21 tumors showed a papillary growth pattern: a feature typically associated with a luminal-like phenotype [31,36]. A prior study reported IHC based molecular subtyping of 15 sarcomatoid tumors and did not identify the same strong trend toward a basal-like phenotype [18]. However, there are clear differences in study design, including the fact that our study specifically included urothelial MIBC with adjacent sarcomatoid morphology. Nevertheless, it is plausible, based on this prior study, that a minority of MIBC with urothelial and adjacent sarcomatoid growth pattern may have a luminal-like phenotype.

A growing body of evidence suggests that intratumoral heterogeneity affects successful cancer treatment [37–39]. This is in line with findings from our study. Intratumoral heterogeneity was apparent between both morphologies and our DRSs of potentially promising drugs clustered the tumors into urothelial and sarcomatoid morphologies. In addition, in 1 urothelial morphology but not the sarcomatoid, we identified a CCND1 amplification in combination with a homozygous loss in CDKN2A. This combination of genomic alterations is thought as a strong sensitizer for CDK4/6 inhibitors that may be promising in the urothelial but not the sarcomatoid morphology in this particular case. Therefore, our hypothesis is in line with others, that suggested different treatment regimens dependent on the genomic and transcriptomic landscape [5]. Interestingly, the sarcomatoid morphology showed high drug sensitivity scores for drugs that are being investigated for the treatment of sarcoma and other malignancies [40–43]. Finally, we found an overexpression of PD-L1 in the sarcomatoid morphology. This is in line with an increased PD-L1 expression in sarcomatoid differentiated kidney and lung carcinomas [44,45]) and may suggest a role of checkpoint inhibition as promising compound for successful treatment. However, only clinical trials may confirm these hypotheses.

We are aware of the limitations of our study that are mainly due to its retrospective character. Due to a meticulous selection of patients to allow an enrollment of a homogeneous cohort of MIBC patients with urothelial and adjacent sarcomatoid morphology, we were limited sample size. However, even within the limited number of cases profiled, we observed consistent patterns in both mutation status and gene expression profiles. Expanding this study to profile additional cases or using a larger panel for genomic DNA sequencing would provide additional evidence to confirm our observations.

5. Conclusion

Conventional urothelial and adjacent sarcomatoid morphology of MIBC arise from the same common ancestor. Both morphologies express a basal-like gene expression signature, with the sarcomatoid morphology having an enrichment for EMT pathways. DRSs revealed drugs that are investigated or used in sarcoma therapy. The overexpression of PD-L1 suggests an immune suppressed tumor microenvironment, which may respond favorably to immune checkpoint inhibition.

Author contributions statement

Data collection: Genitsch, Kollàr, Furrer, Vandekerkhove, Annala, Herberts, Gibb, Liu, Davicioni, Wyatt, and Seiler.

Analysis/interpretation: Genitsch, Kollàr, Blarer, Vandekerkhove, Gibb, Wyatt, and Seiler.

Trial design: Genitsch, Kollàr, Seiler.

Manuscript drafting: Genitsch, Kollàr, Vandekerkhove, Gibb, Wyatt, and Seiler.

Manuscript editing: Genitsch, Kollàr, Blarer, Furrer, Vandekerkhove, Pycha, Annala, Herberts, de Jong, Gibb, Liu, Krentel, Davicioni, Wyatt, and Seiler.

Competing financial interests

Employment: Three authors (YL, ED, EG) are employees of GenomeDx Biosciences which funded the gene

expression analysis of the patient cohort and assisted in the bioinformatics data analysis.

The remaining authors have no direct or indirect commercial financial incentive associated with publishing the article.

Supplementary materials

Supplementary material associated with this article can be found, in the online version, at https://doi.org/10.1016/j.urolonc.2019.06.021.

References

[1] Stein JP, Lieskovsky G, Cote R, Groshen S, Feng AC, Boyd S, et al. Radical cystectomy in the treatment of invasive bladder cancer: long-term results in 1,054 patients. J Clin Oncol 2001;19(3):666–75.

[2] Seiler R, von Gunten M, Thalmann GN, Fleischmann A. Extracapsular extension but not the tumour burden of lymph node metastases is an independent adverse risk factor in lymph node-positive bladder cancer. Histopathology 2011;58(4):571–8.

[3] Advanced Bladder Cancer Meta-analysis Collaboration. Neoadjuvant cisplatin for advanced bladder cancer. Lancet 2003;361(9373):1927–34.

[4] Bellmunt J, de Wit R, Vaughn DJ, Fradet Y, Lee JL, Fong L, et al. Pembrolizumab as second-line therapy for advanced urothelial carcinoma. N Engl J Med 2017;376(11):1015–26.

[5] Robertson AG, Kim J, Al-Ahmadie H, Bellmunt J, Guo G, Cherniack AD, et al. Comprehensive molecular characterization of muscle-invasive bladder cancer. Cell 2017;171(3):540−556.e25.

[6] Sjödahl G, Eriksson P, Liedberg F, Höglund M. Molecular classification of urothelial carcinoma: global mRNA classification versus tumour-cell phenotype classification. J Pathol 2017;242(1):113–25.

[7] Thomsen MBH, Nordentoft I, Lamy P, Vang S, Reinert L, Mapendano CK, et al. Comprehensive multiregional analysis of molecular heterogeneity in bladder cancer. Sci Rep 2017;7(1):11702.

[8] Hovelson DH, Udager AM, McDaniel AS, Grivas P, Palmbos P, Tamura S, et al. Targeted DNA and RNA sequencing of paired urothelial and squamous bladder cancers reveals discordant genomic and transcriptomic events and unique therapeutic implications. Eur Urol 2018;74(6):741–53.

[9] Humphrey PA, Moch H, Cubilla AL, Ulbright TM, Reuter VE. The 2016 WHO classification of tumours of the urinary system and male genital organs—part b: prostate and bladder tumours. Eur Urol 2016;70(1):106–19.

[10] Mitra AP, Fairey AS, Skinner EC, Boorjian SA, Frank I, Schoenberg MP, et al. Implications of micropapillary urothelial carcinoma variant on prognosis following radical cystectomy: a multi-institutional investigation. Urol Oncol 2019;37(1):48–56.

[11] Abufaraj M, Foerster B, Schernhammer E, Moschini M, Kimura S, Hassler MR, et al. Micropapillary urothelial carcinoma of the bladder: a systematic review and meta-analysis of disease characteristics and treatment outcomes. Eur Urol 2019;75(4):649–58.

[12] Metcalfe MJ, Ferguson JE, Li R, Xiao L, Guo CC, Czerniak BA, et al. Impact of high-risk features and effect of neoadjuvant chemotherapy in urothelial cancer patients with invasion into the lamina propria on transurethral resection in the absence of deep muscle invasion. Eur Urol Focus 2017;3(6):577–83.

[13] Vetterlein MW, Wankowicz SAM, Seisen T, Lander R, Löppenberg B, Chun FKH, et al. Neoadjuvant chemotherapy prior to radical cystectomy for muscle-invasive bladder cancer with variant histology. Cancer 2017;123(22):4346–55.

[14] Guo CC, Dadhania V, Zhang L, Majewski T, Bondaruk J, Sykulski M, et al. Gene expression profile of the clinically aggressive micropapillary variant of bladder cancer. Eur Urol 2016;70(4):611–20.

[15] Tschui J, Vassella E, Bandi N, Baumgartner U, Genitsch V, Rotzer D, et al. Morphological and molecular characteristics of HER2 amplified urothelial bladder cancer. Virchows Arch 2015;466(6):703–10.

[16] Ching CB, Amin MB, Tubbs RR, Elson P, Platt E, Dreicer R, et al. HER2 gene amplification occurs frequently in the micropapillary variant of urothelial carcinoma: analysis by dual-color in situ hybridization. Mod Pathol 2011;24(8):1111–9.

[17] Al-Ahmadie HA, Iyer G, Lee BH, Scott SN, Mehra R, Bagrodia A, et al. Frequent somatic CDH1 loss-of-function mutations in plasmacytoid variant bladder cancer. Nat Genet 2016;48(4):356–8.

[18] Warrick JI, Sjödahl G, Kaag M, Raman JD, Merrill S, Shuman L, et al. Intratumoral heterogeneity of bladder cancer by molecular subtypes and histologic variants. Eur Urol 2019;75(1):18–22.

[19] Amin MB. Histological variants of urothelial carcinoma: diagnostic, therapeutic and prognostic implications. Mod Pathol 2009;22(Suppl 2):S96–S118.

[20] Wright JL, Black PC, Brown GA, Porter MP, Kamat AM, Dinney CP, et al. Differences in survival among patients with sarcomatoid carcinoma, carcinosarcoma and urothelial carcinoma of the bladder. J Urol. 2007;178(6):2302–7.

[21] Cheng L, Zhang S, Alexander R, MacLennan GT, Hodges KB, Harrison BT, et al. Sarcomatoid carcinoma of the urinary bladder. Am J Surg Pathol 2011;35(5):e34–46.

[22] Armstrong AB, Wang M, Eble JN, MacLennan GT, Montironi R, Tan PH, et al. TP53 mutational analysis supports monoclonal origin of biphasic sarcomatoid urothelial carcinoma (carcinosarcoma) of the urinary bladder. Mod Pathol 2009;22(1):113–8.

[23] Sung MT, Wang M, MacLennan GT, Eble JN, Tan PH, Lopez-Beltran A, et al. Histogenesis of sarcomatoid urothelial carcinoma of the urinary bladder: evidence for a common clonal origin with divergent differentiation. J Pathol 2007;211(4):420–30.

[24] Ikegami H, Iwasaki H, Ohjimi Y, Takeuchi T, Ariyoshi A, Kikuchi M. Sarcomatoid carcinoma of the urinary bladder: a clinicopathologic and immunohistochemical analysis of 14 patients. Hum Pathol 2000;31(3):332–40.

[25] Vandekerkhove G, Todenhöfer T, Annala M, Struss WJ, Wong A, Beja K, et al. Circulating tumor DNA reveals clinically actionable somatic genome of metastatic bladder cancer. Clin Cancer Res 2017;23(21):6487–97.

[26] Annala M, Vandekerkhove G, Khalaf D, Taavitsainen S, Beja K, Warner EW, et al. Circulating tumor DNA genomics correlate with resistance to abiraterone and enzalutamide in prostate cancer. Cancer Discov 2018;8(4):444–57.

[27] Chedgy EC, Vandekerkhove G, Herberts C, Annala M, Donoghue AJ, Sigouros M, et al. Biallelic tumour suppressor loss and DNA repair defects in de novo small-cell prostate carcinoma. J Pathol 2018;246(2):244–53.

[28] Erho N, Crisan A, Vergara IA, Mitra AP, Ghadessi M, Buerki C, et al. Discovery and validation of a prostate cancer genomic classifier that predicts early metastasis following radical prostatectomy. PLoS One 2013;8(6):e66855.

[29] Seiler R, Ashab HAD, Erho N, van Rhijn BWG, Winters B, Douglas J, et al. Impact of molecular subtypes in muscle-invasive bladder cancer on predicting response and survival after neoadjuvant chemotherapy. Eur Urol 2017;72(4):544–54.

[30] Cancer Genome Atlas Research Network. Comprehensive molecular characterization of urothelial bladder carcinoma. Nature 2014;507(7492):315–22.

[31] Kamoun A, de Reynies A, Allory Y, Sjodahl G, Robertson AG, Seiler R, et al. The consensus molecular classification of muscle-invasive bladder cancer: cancer biology. bioRxiv 2018.

[32] Wang S, Gribskov M, Hazbun TR, Pascuzzi PE. CellMiner companion: an interactive web application to explore CellMiner NCI-60 data. Bioinformatics 2016;32(15):2399–401.

[33] Zlobec I, Suter G, Perren A, Lugli A. A next-generation tissue microarray (ngTMA) protocol for biomarker studies. J Vis Exp 2014:(91):51893.
[34] Ku SY, Rosario S, Wang Y, Mu P, Seshadri M, Goodrich ZW, et al. Rb1 and Trp53 cooperate to suppress prostate cancer lineage plasticity, metastasis, and antiandrogen resistance. Science 2017;355 (6320):78–83.
[35] Boudreau HE, Casterline BW, Burke DJ, Leto TL. Wild-type and mutant p53 differentially regulate NADPH oxidase 4 in TGF-β-mediated migration of human lung and breast epithelial cells. Br J Cancer 2014;110(10):2569–82.
[36] Choi W, Porten S, Kim S, Willis D, Plimack ER, Hoffman-Censits J, et al. Identification of distinct basal and luminal subtypes of muscle-invasive bladder cancer with different sensitivities to frontline chemotherapy. Cancer Cell 2014;25(2):152–65.
[37] da Costa WH, Fares AF, Bezerra SM, Morini MA, de Toledo Benigno LA, Clavijo DA, et al. Loss of BAP1 expression in metastatic tumor tissue is an event of poor prognosis in patients with metastatic clear cell renal cell carcinoma. Urol Oncol 2019;37(1):78–85.
[38] Bedard PL, Hansen AR, Ratain MJ, Siu LL. Tumour heterogeneity in the clinic. Nature 2013;501(7467):355–64.
[39] Meacham CE, Morrison SJ. Tumour heterogeneity and cancer cell plasticity. Nature 2013;501(7467):328–37.
[40] Kunos CA, Chu E, Beumer JH, Sznol M, Ivy SP. Phase I trial of daily triapine in combination with cisplatin chemotherapy for advanced-stage malignancies. Cancer Chemother Pharmacol 2017;79(1):201–7.
[41] Goss KL, Gordon DJ. Gene expression signature based screening identifies ribonucleotide reductase as a candidate therapeutic target in Ewing sarcoma. Oncotarget 2016;7(39):63003–19.
[42] Feleszko W, Mlynarczuk I, Balkowiec-Iskra EZ, Czajka A, Switaj T, Stoklosa T, et al. Lovastatin potentiates antitumor activity and attenuates cardiotoxicity of doxorubicin in three tumor models in mice. Clin Cancer Res 2000;6(5):2044–52.
[43] Kim JS, Pirnia F, Choi YH, Nguyen PM, Knepper B, Tsokos M, et al. Lovastatin induces apoptosis in a primitive neuroectodermal tumor cell line in association with RB down-regulation and loss of the G1 checkpoint. Oncogene 2000;19(52):6082–90.
[44] Kawakami F, Sircar K, Rodriguez-Canales J, Fellman BM, Urbauer DL, Tamboli P, et al. Programmed cell death ligand 1 and tumor-infiltrating lymphocyte status in patients with renal cell carcinoma and sarcomatoid dedifferentiation. Cancer 2017;123(24):4823–31.
[45] Vieira T, Antoine M, Hamard C, Fallet V, Duruisseaux M, Rabbe N, et al. Sarcomatoid lung carcinomas show high levels of programmed death ligand-1 (PD-L1) and strong immune-cell infiltration by TCD3 cells and macrophages. Lung Cancer 2016;98:51–8.